CONSTITUTIVE MODELING OF FORCE-CONTROLLED FATIGUE TESTING IN HUMAN MENISCUS TISSUE

by

Bradley Scott Henderson

A thesis

submitted in partial fulfillment

of the requirements for the degree of

Master of Science in Mechanical Engineering

Boise State University

December 2020

BOISE STATE UNIVERSITY GRADUATE COLLEGE

DEFENSE COMMITTEE AND FINAL READING APPROVALS

of the thesis submitted by

Bradley Scott Henderson

Thesis Title: Constitutive Modeling of Force-Controlled Fatigue Testing in Human Meniscus Tissue

Date of Final Oral Examination: 20 November 2020

The following individuals read and discussed the thesis submitted by student Bradley Scott Henderson, and they evaluated their presentation and response to questions during the final oral examination. They found that the student passed the final oral examination.

Trevor Lujan, Ph.D.	Chair, Supervisory Committee
Clare Fitzpatrick, Ph.D.	Member, Supervisory Committee
Mahmood Mamivand, Ph.D.	Member, Supervisory Committee
Zhangxian Deng, Ph.D.	Member, Supervisory Committee

The final reading approval of the thesis was granted by Trevor Lujan, Ph.D., Chair of the Supervisory Committee. The thesis was approved by the Graduate College.

DEDICATION

This thesis is dedicated to my family, especially my mother, for their unconditional support. Samantha Hanson for always believing in me, and to my closest friends for constantly keeping a smile on my face.

ACKNOWLEDGMENTS

I would like to acknowledge my thesis advisor Dr. Trevor Lujan, and all my lab mates in the Northwest Tissue Mechanics laboratory. Most of all, Katelyn Cudworth, Danielle Siegel, and Maddison Wale for their contributions to the experimental section of this study. I would also like to thank all of the donors who allowed their knees joints post-mortem to be used for research making these studies possible, and Bella Vita Funeral Home (Garden City, ID) for their help in laying donors to rest. Financial support for this research was provided by the National Science Foundation under grant no. 1554353 and the NIGMS award no. P20GM109095.

ABSTRACT

The meniscus is a wedge-shaped fibrocartilaginous tissue located between the femur and tibia that helps stabilize the knee and protect the underlying cartilage. There are 2.5 million reported knee injuries each year, making it the most injured joint in the human body. Nearly twenty percent of these injuries are due to a torn meniscus, leading to over half a million meniscus surgeries performed in the United States annually. Therefore, it is critical to understand the failure modes of meniscus tissue to prevent these debilitating injuries. A failure mode that accounts for one-third of all meniscus injuries is repeated exposure to low-magnitude tensile loads, known as fatigue. One approach to gain physical insight into fatigue mechanisms is through cyclic tensile experiments performed in laboratories. An alternative approach is to use constitutive mathematical models that predict and describe the material's behavior. These models can avoid the expense and time required for experimental fatigue studies, but they also must be calibrated and validated using experimental data.

The aim of this study is to validate a constitutive model to predict human meniscus' observed fatigue behavior in force-controlled loading. Three variations of constitutive models were applied to test each model's ability to model fatigue induced creep. These models included a viscoelastic damage model, a continuum damage mechanics model, and a viscoelastic model. Using a custom program, each models' parameters were fit to stretch-time plots from previously performed fatigue experiments of cadaveric human meniscus. The quality of fit for each model was then measured.

The results of this study show that a viscoelastic damage formulation can effectively fit force-controlled fatigue behavior and, on average, performed the best of the three models presented. On average, the resulting NRMSE values for stretch at all creep stages were 0.22%, 2.03%, and 0.45% for the visco-damage, damage-only, and visco-only models, respectively. The requirement of including both viscoelasticity and damage to model all three creep stages indicates that viscoelasticity may be the driving factor for damage accumulation in fatigue loading. Further, the relatively low damage values, ranging from 0.05 to 0.2, right before exponential increases in stretch, indicate that failure may occur from fatigue loading without a considerable accumulation of damage. The validation results showed that the model could not completely represent pull to failure experiments when using material parameters that curve fit fatigue experiments. Still, they indicated that the combination of discontinuous CDM and viscoelasticity shows potential to model both fatigue and static loadings using a single formulation. To our knowledge, this is the first study to model force-controlled fatigue induced creep in the meniscus or any other soft tissue. This study's results can be utilized to further model force-controlled fatigue to predict and prevent meniscus tissue injuries.

TABLE OF CONTENTS

LIST OF TABLES

LIST OF FIGURES

CHAPTER ONE: INTRODUCTION

1.1 Motivation

The meniscus is a wedge-shaped fibrocartilaginous tissue located within the knee joint. The meniscus's primary functions are to act as a shock absorber between the tibia and femur and to reduce localized regions of stress by distributing loads. Injuries to the meniscus tissue, which account for nearly twenty percent of all knee injuries, may result in tears. These tears lead to over half a million meniscus surgeries performed in the United States annually. Once torn, the meniscus may become less effective in distributing joint loads, resulting in increased damage to the articular cartilage that covers the femur. The resulting irreversible damage to the knee joint may lead to osteoarthritis, a debilitating and irreversible disease, that affects millions worldwide. Thus, it is critical to gain a deeper understanding of the failure modes which produce these tears.

A failure mode that may be responsible for one-third of meniscus injuries is the repeated exposure to low magnitude loads known as fatigue (Demange et al., 2015). Fatigue is commonly studied in the laboratory through cyclic experimentation and has been well quantified for conventional materials; however, this failure mode has only been recently studied for human meniscus and other musculoskeletal tissue. Further, these experiments require a significant amount of resources due to their high cost and time requirements. An alternative approach commonly used for conventional materials is to utilize material constitutive models that describe the relationship between stress, strain,

and internal state variables. However, to our knowledge, no such model exists for force-controlled fatigue of meniscus or any other soft tissue.

The verification and validation of such a model would lead to a deeper understanding of the physical workings of force-controlled fatigue in meniscus tissue. The determination of constitutive equations and their combinations that can effectively reproduce fatigue data can also give mathematical insight into what causes fatigue phenomena including creep and failure. Ultimately, this information can be used to inform and develop new techniques relating to the prevention and treatment of soft tissue injury.

1.2 Research Goal

This study's primary objective was to determine a mathematical formulation that can describe meniscus tissue's physical response to force-controlled fatigue testing. The formulations investigated included a viscoelastic damage model, a continuum damage mechanics model, and a viscoelastic model. Experimental and computational methods were utilized to accomplish the research goal. Force-controlled fatigue experiments were previously conducted to measure the high-cycle tensile fatigue behavior in meniscus tissue. The resulting experimental data was used to fit specimen-specific material parameters for the three constitutive equations investigated using a least-squares algorithm. The material parameters and constitutive equations were numerically used to determine axial and lateral stretch values, given the constant input load. The resulting axial stretch was compared to the experimental creep curve to determine the efficacy of the model. It was hypothesized that the viscoelastic damage model would best predict meniscus tissue's mechanical response to force-controlled fatigue experiments.

CHAPTER TWO: BACKGROUND

2.1 Meniscus Structure and Function

The meniscus is a fibrocartilaginous tissue consisting of a medial and lateral component, located between the femoral condyle and tibial plateau (Kohn and Moreno, 1995). The tissue has a unique crescent moon shape with a wedge profile (Clark and Ogden, 1983) (Figure 1). The meniscus is highly hydrated in physiological conditions comprising of roughly 72% water. The remaining 28% is the extracellular matrix (ECM) (Herwig et al., 1984) that consists of proteoglycan and collagen. Proteoglycans are proteins attached to long linear polysaccharide chains known as glycosaminoglycans (GAGs). Most of the collagen that makes up meniscus tissue is type one and is found as circumferentially aligned fibers that are responsible for the tensile strength of the tissue and play a critical role in the meniscus function.

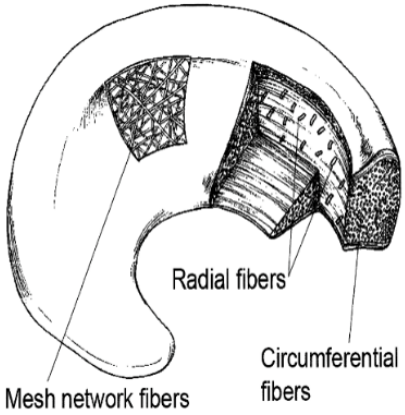

Figure 1. The meniscus tissue structure (Bullough et al., 1970).

The main function of the meniscus is to distribute approximately 20% of the stress between the tibia and femur bones (Voloshin and Wosk, 1983). The meniscus' unique wedge shape stabilizes the knee joint and converts compressive loads delivered to the tissue to circumferential hoop stress (Sweigart and Athanasiou, 2001, Hoshino and Wallace, 1987, Radin et al., 1984) (Figure 2) resulting in essential tensile stresses along the direction of the circumferential fibers.

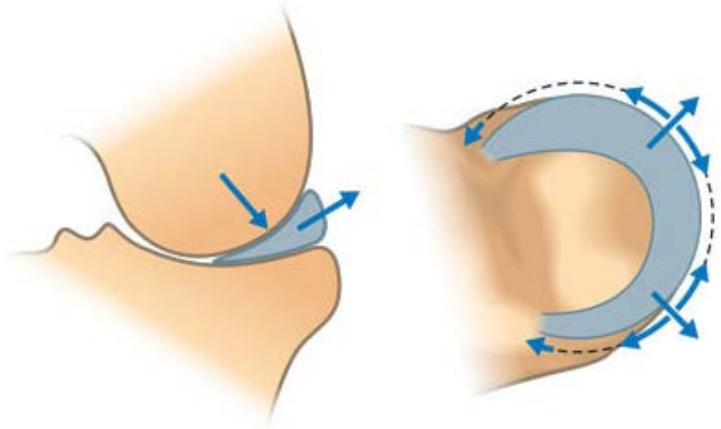

Figure 2. Compressive load delivered to the meniscus resulting in circumferential hoop stress (Total Meniscus Replacement Technology, 2017).

Tensile stresses can result in damage to the circumferential fibers ultimately causing tears. Complex tears in the meniscus can be very difficult to treat due to the tissues avascularity resulting in limited natural healing abilities (Clark and Ogden, 1983). The current accepted treatment approach is partial meniscectomy, leading to long-term implications for the underlying cartilage (Roos et al., 2001) and limiting the functionality of the remaining meniscus tissue. The meniscus' role in load distribution is essential to prevent damage to cartilage that increases the risk of osteoarthritis (OA), a degenerative and irreversible disease, resulting in tremendous pain and function loss.

2.2 Mechanical Fatigue Testing

Soft tissues are likely to fail in one of two main ways. The first, known as static failures, are caused by a single high-magnitude event. These are commonly sport-related and tend to occur in younger aged populations (Snoeker et al., 2013). This failure category is well defined in the literature and accounts for two-thirds of meniscal tears (Demange et al., 2015). The second failure mode is due to low-magnitude repeated loads, known as fatigue. Unlike static failure, these injuries are not related to traumatic events or previous illnesses and commonly occur in older populations. Although fatigue has been reported to account for one-third of all meniscal failures (Demange et al., 2015), it is still not well understood, resulting in a lack of knowledge in the current literature regarding mechanisms that cause fatigue phenomena including creep and failure. Mechanical fatigue testing and analysis can be performed to quantify fatigue characteristics filling this gap.

Fatigue characteristics are caused by low magnitude, repeated loads applied to a material. This cyclic loading results in damage accumulation, which leads to softening of the material. As the material softens, more strain is required to maintain constant peak stress. This increase in displacement is known as creep. Creep can be described in three principal regions. The first occurring, known as the primary response, is a drastic increase in strain due to an applied load, which, when held constant, results in a reduction of strain rate with time. The secondary, or steady-state, creep then begins, and the strain rate becomes constant. After enough damage has occurred, the tertiary stage starts where the material begins to exponentially deform until rupture occurs. There are three main testing

methods used to analyze fatigue induced behavior: the strain-life method, linear elastic fracture mechanics, and the stress-life method.

The strain-life method is typically used to characterize low-cycle fatigue ($<10^4$ cycles) in which high cyclic displacements are applied to induce plastic strain. This loading scenario is not physiological to soft tissue as fatigue of these materials typically happens from low-magnitude stresses that occur before plastic deformation and thus this method is not further discussed.

The linear elastic fracture mechanics method describes fatigue by studying crack propagation. This requires the assumption that a crack exists even if microscopic. The crack growth can then be monitored until it reaches a critical size for the stress amplitude applied, when sudden, catastrophic failure occurs. By performing many tests on the same material at various stress amplitudes, material constants can be determined and used to predict a material's remaining cycle life given an initial crack size. This method is useful when studying traditional materials like metals but is not practical for soft tissues. Initial crack size in soft tissues is difficult to measure if they are detectable at all. Some studies have induced tears before testing the tissue to overcome this issue, hindering its mechanical integrity (Peloquin and Elliott, 2016). This results in quantifying properties that are not native to the tissue and thus less useful clinically. Due to the presented limitations regarding this method’s use for soft tissue it is not further discussed.

The third approach to quantify fatigue behavior is the stress-life method. This method is used for high cycle fatigue ($>10^4$ cycles) and is therefore more physiologically relevant for characterizing soft tissue. This method is performed by cyclically applying various stress levels, defined as a percentage of the ultimate tensile strength (UTS), to a

material. The amount of cycles required to cause failure at the corresponding %UTS is then quantified. The cycles to failure, N, and %UTS pairs can then be plotted and interpolated to produce an S-N curve. S-N curves are used to predict the cyclic lifetime of a material given an applied stress. Further, these curves can determine if an endurance limit, a stress level at which failure will never occur regardless of cycle number, exists for a given material. Endurance limits have been discovered in metals but have never been studied for meniscus or other soft fibrous tissues. For traditional materials, like metals, these tests are commonly performed in a tension-compression sequence resulting in a fully reversible load. Although this is characteristic of objects such as metal shafts, it does not represent soft tissue's natural loading. Thus, studies performing fatigue testing on soft tissue, including ligament and bovine meniscus, have used a tension-tension loading profile. Due to its physiological relevance and previous usage for soft tissue in literature, a tension-tension stress-life method is most applicable for the investigation of fatigue behavior in meniscus tissue.

2.3 Constitutive Models for Fatigue

Constitutive models can be defined as a mathematical representation of complex physical behavior using simplified formulations. Although these models are constantly being expanded upon for improved accuracy, no exact model exists. Constitutive models are used in mechanical analysis to describe and predict mechanical behavior of materials under various loading conditions. The most common relationship described in mechanics using constitutive equations is the coupling of stress and strain. Engineers can utilize and develop constitutive models to find an effective yet simple and efficient representation of a mechanical observation.

There have been a few major approaches to constitutive modeling using continuum theory regarding the description of the macro-scale mechanical behavior of materials. If a material's behavior has been described through experimental observation, two main formulations can be used. The first category, known as phenomenological models, uses the development of equations with no physical basis (e.g. quadratic curve fitting). The second method, known as physical models, is based upon the first principles (e.g. conservation of mass) and structural characteristics. Due to the physical characteristics of some of the material parameters gained through curve-fitting, the focused modeling approach to describe observed mechanical behavior, for this research, is a combination of both phenomenological and physical modeling.

This modeling combination can describe the many different mechanical behaviors materials display based on the loading conditions presented and their structural makeup. Typical behaviors studied and modeled include elasticity, material response before any permanent deformation without time dependency, viscoelasticity, representing time dependency, and plasticity, material response after permanent deformation. Material failure for cyclic loading is typically modeled using continuum damage mechanics (CDM), representing material softening, or fracture mechanics, describing crack propagation.

For force-controlled fatigue testing of soft tissues, CDM may be applied to represent the cyclic softening of the material due to the elastic loads applied. This theory reduces the nominal stress to an effective stress using a scalar damage variable *d*. The damage variable represents some amount of material area that no longer can take any stress (Figure 3). The variable ranges from zero to one, and when equal to one represents

complete failure of the material. The damage evolution is governed by a damage criterion which is commonly energy based and determines when and how damage accumulates.

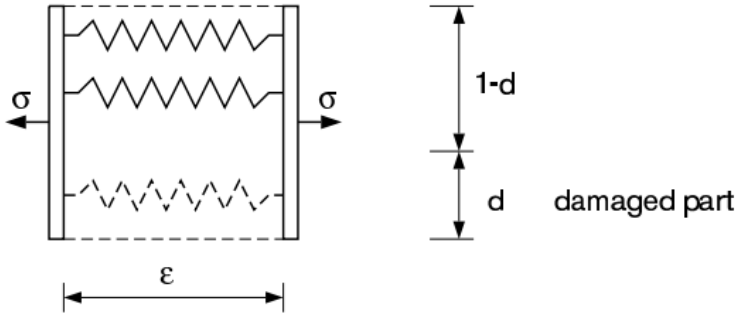

Figure 3. An elementary model of elastic damage based on the equivalent strain principle (Runesson, 2006).

Force-controlled fatigue experiments also display time-dependent deformation and thus viscoelasticity is applicable. Viscoelasticity can be modeled using various theories. One of the most common is quasi-linear viscoelasticity (QLV) where previous events are accounted for using a convolution integral and a relaxation function. As the event becomes further from the current time it has less effect on the current response of the material. The relaxation functions use parameters which determine how quickly the material relaxes to its long-term elastic response. These parameters may be determined by curve-fitting to experimental data.

For rubber-like materials, cyclic loading can be modeled using damage coupled to viscoelasticity. This formulation can represent typical behavior of soft tissues under this loading criteria including hysteresis, softening, and failure (Figure 4).

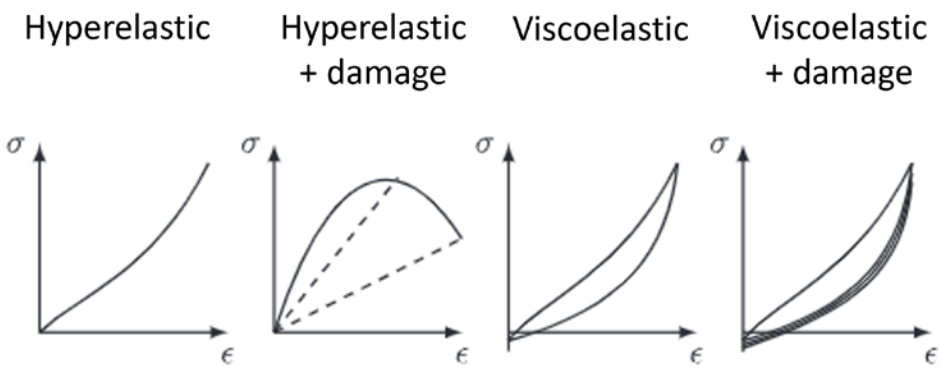

Figure 4. The constitutive response of rubber-like materials under cyclic loading (Jha et al., 2019).

Although coupling of damage and viscoelasticity has been shown to be effective for modeling cyclic behavior for rubber-like materials such as soft-tissues, it has never been shown to model fatigue induced creep for human meniscus or any other soft tissue in a force-controlled experiment and is thus the focus of this study.

2.4 Computational Methods for Simulating Constitutive Models

To describe the behavior of materials using constitutive models, analytical and numerical methods can be utilized to solve constitutive equations. Analytical solutions give exact results governed by underlying assumptions such as small displacements or the material having an elastic stress-strain behavior. Analytical models regarding meniscus developed in previous studies commonly make assumptions, including that the tissue is linearly elastic and has a linear viscoelastic media (Imeni et al., 2020). To avoid drastic assumptions and to apply more complex and accurate constitutive models, numerical methods can be used to achieve an estimate, with a very high tolerance, to predict material behavior. This is commonly done using either finite element analysis (FEA) or optimization frameworks (Imeni et al., 2020).

Open-source software such as FEBio, a nonlinear analysis tool used for biomechanics, and WARP3D, a nonlinear analysis tool focused on fatigue and fracture analysis in metals, utilize FEA to solve a wide variety of user inputted problems. FEA can solve large, complex problems by subdividing the system into smaller pieces called finite elements. Each finite element (FE) is described using a local equation, which defines the total solution when combined into a set. The system of equations is then solved by minimizing the error associated with trial solutions. Although FEA is very popular and commonly utilized by engineers to model material behavior, it has some significant limitations when modeling force-controlled fatigue behavior of soft tissues. Force-controlled FEA problems are inherently unstable (FEBio, n.d.) due to small but not negligible errors associated with approximations of solutions. Even the slightest numerical round-off can cause a misbalance of forces and thus the divergence of a model (FEBio, n.d.). Another limitation of FEA modeling of soft tissues is material instability due to material softening. This issue becomes apparent at large deformations when the tangent modulus of the material becomes or nears zero, which leads to the solver needing to take an infinite step to find a solution. These limitations can be overcome by using optimization frameworks.

When experimental data is available constitutive models can be solved through optimization techniques using a least-squares approach. This approach minimizes an objective function defined as the sum of the squared difference between the observed and modeled values of the dependent variable. To find the independent variable that minimizes the objective function, an iterative approach is used, such as the Levenberg-Marquardt algorithm (LMA). The least-squares approach is effective in modeling force-

controlled fatigue by determining stretches, given a constitutive model and experimental force data, overcoming the previous limitations discussed for analytical and FEA solutions.

CHAPTER THREE: CONSTITUTIVE MODELING OF FORCE-CONTROLLED FATIGUE TESTING IN HUMAN MENISCUS TISSUE[1]

3.1 Introduction

The meniscus is a wedge-shaped fibrocartilaginous tissue located between the femur and tibia that plays a crucial role in joint health yet is also frequently injured. By distributing and dissipating large and repeated loads, the meniscus reduces localized regions of stress that can damage the underlying articular cartilage, increasing the risk of osteoarthritis (Fox et al., 2012; Hutchinson et al., 2013). Injuries due to a torn meniscus, lead to over half a million meniscus surgeries performed in the United States annually (Kim et al., 2011). As many as one-third of meniscus injuries may be caused by repeated exposure to low-magnitude loads, known as fatigue (Demange et al., 2015). Compressive loads delivered to the knee are converted to hoop stress within the meniscus tissue putting the circumferential fibers in cyclic tension. Fibers display time-dependent viscoelastic behavior to repeated stresses until tissue rupture, known as fatigue creep (Figure 5). Fatigue creep behavior can be described in three principal regions. The tissue's primary response is an increase in stretch due to cyclic loading shown in stage I (Figure 5). This leads to softening of the material resulting in higher stretch values for the same loads applied. The rate of weakening is greatest during the initial loading and then enters a

[1]This chapter will be submitted for publication

steady-state phase indicated in stage II (Figure 5). As the material continues to be gradually stretched and softening continues, the increases in stretch eventually become non-linear, stage III, where displacement values quickly rise until tissue rupture (Figure 5). While the study of fatigue in conventional materials has been transformative to the engineering and maintenance of durable polymers and composites, there is a fundamental lack of knowledge on the structural mechanisms of fatigue failure in fibrous soft tissue.

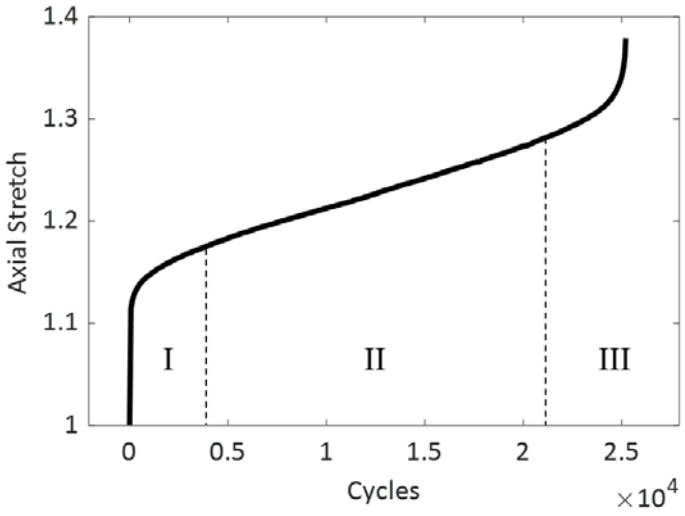

Figure 5. Fatigue induced creep response to a constant cyclic force. Creep can be categorized into three stages: I) the rapid response to initial cyclic loading, II) the steady-state stage, and III) the exponential increase in stretch up to failure.

A proven approach to gain physical insight into fatigue mechanisms is through mathematical constitutive models that predict and describe material damage. These models can avoid the expense and time required for experimental fatigue studies, but they also must be calibrated and validated using experimental data. A few constitutive frameworks that have had success in simulating the damage processes of soft biological tissue include continuum damage mechanics (CDM) (Martin and Sun, 2012, Pena, 2011, Balzani et al., 2012), pseudoelasticity (Franceschini et al., 2006), and elasto-

viscoplasticity (Zhu, 2018) to account for stress softening and permanent set effects. Notably, most of these models have been validated with experiments that use displacement control loading, where a cyclic strain is applied, and stress reduces overtime. A loading condition that is more physiological to joint kinetics and fatigue injury is repeated application of a targeted stress (force-control). However, to our knowledge, no computational study has modeled force-control fatigue data in the meniscus, or any other musculoskeletal soft tissue.

A novel and elegant solution for modeling cyclic creep behavior in soft tissue may be possible using discontinuous CDM with viscoelasticity. Discontinuous CDM is physically described as the deterioration of mechanical properties due to damage from a material being deformed beyond its elastic limit, where mathematically, damage evolves when a specified failure criterion is exceeded. Previous work has determined that discontinuous CDM with strain energy-based failure criteria can model quasi-static failure in soft tissue (Martin and Sun, 2017), but discontinuous CDM has intrinsic limitations in modeling force-controlled fatigue loading since damage evolution is restricted under a constant load. Viscoelastic models describe both the elastic and viscous behavior of materials using time-dependency. Viscoelasticity can represent steady state creep (stage II) (Sopakayang and Vita, 2011), but is unable to model damage propagation to material rupture (stage III). By pairing a discontinuous, strain-energy based, CDM model with a viscoelastic model, it may be possible for damage to propagate in response to viscoelastic creep during a force-controlled experiment. In this way, the individual limitations of each model type can be overcome, and potentially both fatigue and static loading could be modeled using a single formulation.

The objective of this study is to determine the feasibility of using CDM and viscoelastic models to simulate high-cycle tensile loading in human meniscus. The CDM and viscoelastic models will be tested both individually and combined. It is hypothesized that the interplay of energy based CDM and viscoelasticity will result in the best prediction of cyclic creep behavior. If this hypothesis is supported, the model would give insight into how material failure propagates in meniscus, and other soft tissue.

3.2 Methods

3.2.1 Overview

An experimental and computational approach was used to address the study objective. Nine dumbbell-shaped specimens from five human menisci were mechanically tested in cyclic tension to characterize fatigue creep behavior at three different stress levels (30, 50, and 70% of UTS). The stress and stretch data from these experiments was used to calibrate the subject-specific material parameters for three constitutive models: visco-damage, damage-only, and visco-only. The calibration of material parameters was performed in a custom MATLAB code that simulated a single three-dimensional cube subjected to force-controlled loading. The quality of the curve fit for each model was quantified using normalized root mean square error (NRMSE). The ability of the calibrated models to predict experimental data not used for curve fitting (i.e. model validation) was evaluated using test data from quasi-static uniaxial tests to failure. A sensitivity analysis was performed to determine the effect of the material parameters on the resulting creep behavior.

3.2.2 Mechanical Testing

Medial menisci were obtained from five unpaired human fresh frozen cadaveric knee joints (femur to tibia) from young donors (age = 32±6 years; 4 male and 2 female). All knees had no medical history of injury and all menisci did not display any degenerative fraying. Knee joints were stored at -20C and were allowed to thaw at room temperature for at least 24 hours prior to dissection. The medial meniscus was excised, sectioned into anterior and posterior regions, embedded in Celluclay, and sliced into ~0.8 mm thick layers along the circumferential-axial plane with a commercial deli-slicer (Globe, Bridgeport CT; Model C12). Layers were then cut into dumbbell-shaped geometry using custom 3D-printed punches with bendable razors (Nelson et al., 2020). The long axis of the punch was aligned in the direction of the preferred circumferential fiber orientation.

Prior to fatigue testing, quasi-static uniaxial tensile tests to failure were performed on eight dumbbell shaped specimens from five knees to generate a correlation between tangent modulus and ultimate tensile strength. This allowed for the non-destructive prediction of UTS from modulus data. All tensile tests were performed in a saline tank (Test Resources, Shakopee MN; T200 Bath Controller; Temp Control ± 0.2C) using an electrodynamic mechanical testing system (Instron, Norwood MA; Electropuls E10000) (Figure 6A). Before inserting the test coupons into test fixtures, emery cloth tabs were bonded with cyanoacrylate to the coupon ends to help prevent slipping. After preloading to 0.1 N, specimen dimensions were measured using digital images of the dumbbell-shaped coupon (Figure 6B) (Creechley et al., 2017). The specimens were then buckled, and the tank was filled with 0.9% saline solution at 37C (Figure 6A). Specimens were

then preloaded a second time to 0.1 N, preconditioned with a 20-cycle triangular wave to 8% clamp strain, and pulled to failure at 1% strain/s. Tangent modulus and UTS were measured using established methods (Wale et al., 2020), and these material properties were correlated with linear regression (Figure 7).

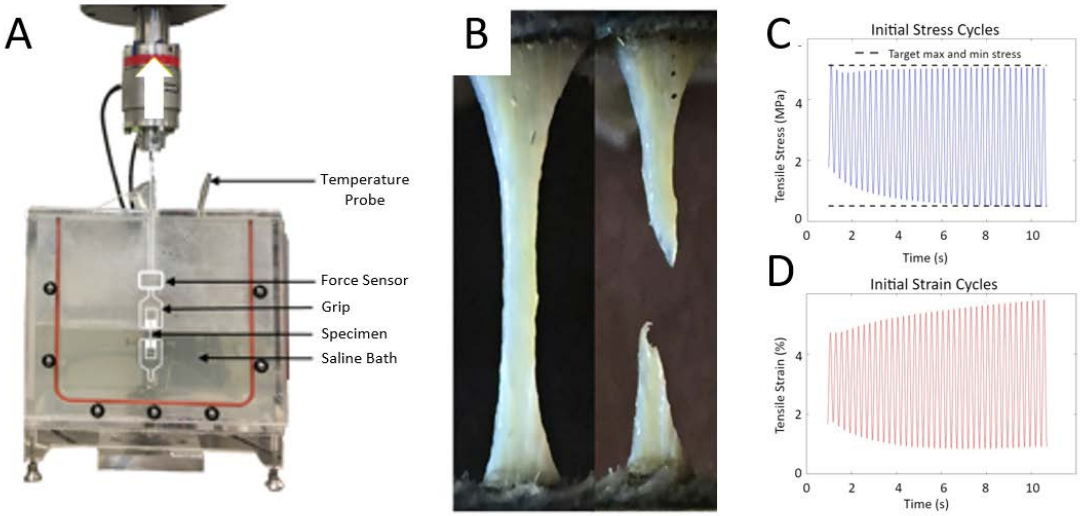

Figure 6. Fatigue experiment. A) Specimen pre- and post-test. B) Apparatus for mechanical testing with direction of cyclic tension indicated in white. C) Start of cyclic loading to target stress and D) resulting strain response.

Tensile fatigue tests were then performed on nine dumbbell shaped specimens from the same set of human menisci used for quasi-static tensile tests to failure. Using the same methods described for the quasi-static tests, emery cloth was adhered to the coupons, specimens were preloaded, imaged for dimensions, buckled, immersed in 37C saline solution that contained 0.05 mg/mL of both penicillin and streptomycin for 1 hour, preloaded to 0.1 N, and preconditioned. For cyclic testing, targeted engineering stress was selected at 30, 50, and 70% of UTS by calculating the tangent modulus from the last cycle of the preconditioning waveforms, and then estimating the UTS from the linear correlation (Figure 7).

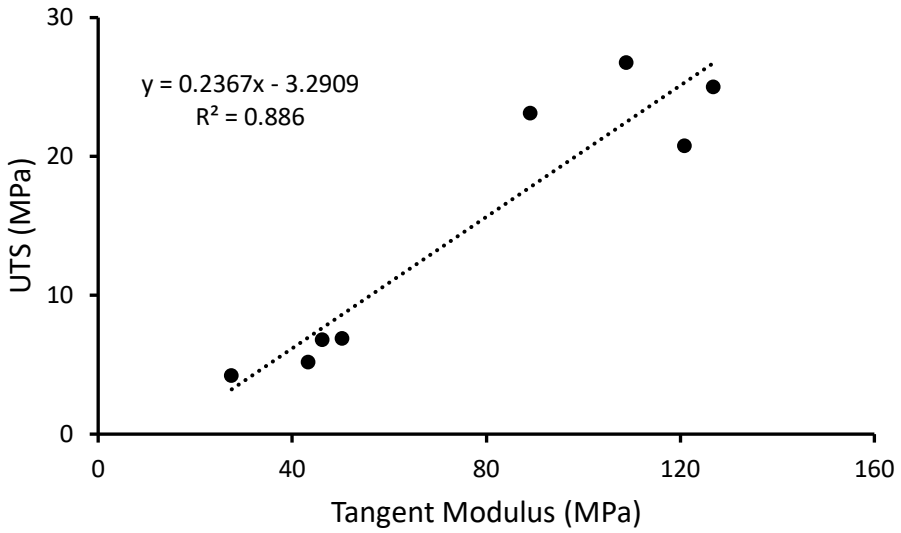

Figure 7. Correlation of UTS and tangent modulus from quasi-static tensile tests. This correlation was used to non-destructively predict the UTS for fatigue specimens by measuring the tangent modulus during preconditioning. Each specimen could then be fatigue tested to a targeted %UTS (30, 50, and 70%).

A 4 Hz tensile-tensile sinusoidal waveform was applied to the targeted stress (minimum = 10% of the targeted stress) until failure or one-million cycles was reached. The measured maximum stress values were within 0.7 +/- 0.7% of targets (Figure 6C). If failure did not occur before one-million cycles, the specimen was pulled to failure in quasi-static tension. All specimen failures occurred away from the grip line, within the midsubstance (Figure 6B), or near the fillet (i.e., width tapered section) (Nesbitt et al., 2020). The cyclic creep curves for each experiment were generated by taking the peak displacement values for each strain cycle (Figure 6D). These values were then converted to stretch and plotted versus cycles.

3.2.3 Constitutive Models

Three constitutive model formulations were investigated: visco-damage, visco-only, and damage-only. The cyclic creep curves from the fatigue experiments were used to calibrate the material parameters for each model.

3.2.3.1 Viscoelastic-Damage Model

The viscoelastic-damage model used a continuum damage mechanics formulation, where the viscoelastic stress response was reduced by a damage variable, *D*, that had a range $0 \leq D \leq 1$, with $D = 1$ representing complete failure. This damage variable scaled the elastic 2nd Piola-Kirchhoff (PK) stress $\mathbf{S}^{\mathrm{e}}$ and the relaxation function *G* by utilizing a quasi-linear viscoelastic formulation through the application of a convolution integral.

$$\mathbf{S}(t) = \int_0^t G(t-s)(1-D(t))\frac{\mathrm{d}\mathbf{S}^{\mathbf{e}}}{\mathrm{d}s}\mathrm{d}s \tag{1}$$

Here, *t* is the current time and *s* represents all incremental time points. The 2nd PK elastic stress $\mathbf{S}^{\mathrm{e}}$ was calculated from a strain energy formulation using the right Cauchy-Green deformation tensor $\mathbf{C}$, which is a function of the deformation tensor $\mathbf{F}$.

$$\mathbf{S}^{\mathrm{e}} = 2\frac{\partial W}{\partial \mathbf{C}} \tag{2}$$

Where, strain energy density, W, was modeled using a Neo-Hookean formulation and is comprised of lamé's first parameter λ, the shear modulus μ, the first scalar invariant I_1, and *J*, the determinant of $\mathbf{F}$.

$$W = \frac{\mu}{2}(I_1 - 3) - \mu \ln J + \frac{\lambda}{2}(\ln J)^2 \tag{3}$$

The relaxation function inside the convolution integral was comprised of six material parameters $\gamma_1, \gamma_2, \gamma_3, \tau_1, \tau_2, \tau_3$ which regulate how quickly the material relaxes to its long-term elastic stress.

$$G(t) = 1 + \gamma_1 e^{\frac{-t}{\tau_1}} + \gamma_2 e^{\frac{-t}{\tau_2}} + \gamma_3 e^{\frac{-t}{\tau_3}} \quad (4)$$

The energy-based Weibull cumulative distribution function (CDF) was used for the damage evolution model. This CDF is dependent on two material parameters: the shape parameter α and the scale parameter μ, where damage is a function of the Simo damage criteria Ξ.

$$D(\Xi) = 1 - e^{-\frac{\Xi^{\alpha}}{\mu}} \quad (5)$$

Where Ξ is a function of the strain energy density, W.

$$\Xi(\mathbf{F}) = \sqrt{2W} \quad (6)$$

This damage function can be described as discontinuous in that it is characterized by a function of maximum strain energy attained in a loading path that can only evolve when the current maximum strain energy value is exceeded.

3.2.3.2 Viscoelastic Model

A viscoelastic model, with no damage, was effectively created by setting the CDF parameters in the previously described visco-damage model to very high values (α=μ=10,000). This kept the damage term D equal to zero for the range of stretches used in this study.

3.2.3.3 Damage Model

A damage model, with no viscoelasticity, was effectively created by setting all six viscoelastic parameters of the relaxation function in the previously described visco-damage model to zero. This forces the viscoelastic response to equal the long-term elastic response and is thus equivalent to a damage model without any viscoelasticity.

3.2.4 Curve Fitting Using a Single Element Model

Constitutive equations are commonly utilized in FE solvers to model global and local mechanical behavior. However, FE solvers have inherent limitations, including instability when modeling force-controlled damage. This loading scenario leads to an ill-conditioned stiffness matrix caused by the material's softening at large deformations. In addition, constitutive equations are not easily formulated for strain and are typically represented for stress as a function of deformation. This means that material parameter optimization for FE software packages are typically limited to displacement control loading, where a displacement is input, and the parameters are fit to a known stress response. Further, displacement control parameter optimization results in different values than calibration in force-control, thus; the computational simulation of the experimental fatigue results requires the calibration of material parameters in force-control loading.

To overcome these limitations, a three-dimensional single element material model was developed in MATLAB (Figure 8). This custom Force Control Optimization (FC-Opt) program consisted of two nested loops. The inner loop used the Levenberg-Marquardt algorithm (LMA; a modified Newton method used for non-linear least-squares optimization) to calculate axial and lateral stretches at each time point for a targeted loading profile (force-control) (Eq 7). To ensure that damage was irreversible, axial stretch was constrained to be either equal or greater than the axial stretch at the prior time step. The outer loop applied LMA to the entire stretch-time profile to optimize the fit of specimen specific material parameters (Eq 8). The FC-Opt program was applied to the previously described viscoelastic-damage constitutive equation, where the total stress state (Eq. 9) was calculated by summing the past (Eq 10) and current stress terms (Eq

11). For the constitutive model, the derivative of the elastic stress was found numerically using a linear approximation. The integral value at each time point was then approximated numerically by summing the product of the argument value and its corresponding time step. After simplification, the stress value was approximated by summing the product of the relaxation function value, damage function value, and the change in elastic stress at each time point.

$$minimize\ \sum_{i=0}^{t}\left(\left(\mathbf{S}_{experiment}(i)-\mathbf{S}_{model\ axial}(i)\right)^2+\mathbf{S}_{model\ lateral}(i)^2\right) \tag{7}$$

$$minimize\ \sum_{i=1}^{t}\left(\lambda_{experiment}(i)-\lambda_{model}(i)\right)^2 \tag{8}$$

$$\mathbf{S}_{model}(i)=\mathbf{S}_{current}(i)+\mathbf{S}_{past}(i) \tag{9}$$

$$\mathbf{S}_{past}(i)=\sum_{j=1}^{i-1}G\left(i-\left(j-\frac{\Delta t}{2}\right)\right)\Delta\mathbf{S}(j) \tag{10}$$

$$\mathbf{S}_{current}(i)=G\left(\frac{\Delta t}{2}\right)\left(\mathbf{S}^e(i)\big(1-D(i)\big)-\mathbf{S}^e(i-1)\big(1-D(i-1)\big)\right) \tag{11}$$

Prior to inputting the experimental data from the cyclic fatigue experiment, the data was reduced to include only the maximum stress and corresponding stretch to reduce computational cost while still quantifying the tissue's cyclic creep behavior. The load data was then smoothed to reduce noise and held constant during the second phase of creep to remove any irregularities due to noise. The data used for, stretch and material parameter, optimization was interpolated to a set number of points to reduce run time. Curved portions of the input profile were weighted with more data points to improve interpolation accuracy and a visual inspection was made to ensure the interpolated data was representative of all portions of the experimental data. Numerical simulations were run for all nine experiments, and the quality of the models' fit to the observed stretch-time behavior was quantified using NRMSE values for each stage of creep (I, II, and III), the total creep (I - III), and the total stress (I - III). The NRMSE values were calculating by

dividing the root mean square error (RMSE) value of each section by the mean value for that section's experimental data set (e.g. stretch data). Any tests resulting in NRMSE values greater than 10% for stress stage I - III for each model was excluded from all analysis. One 70% experiment met this criterion and was excluded from analysis.

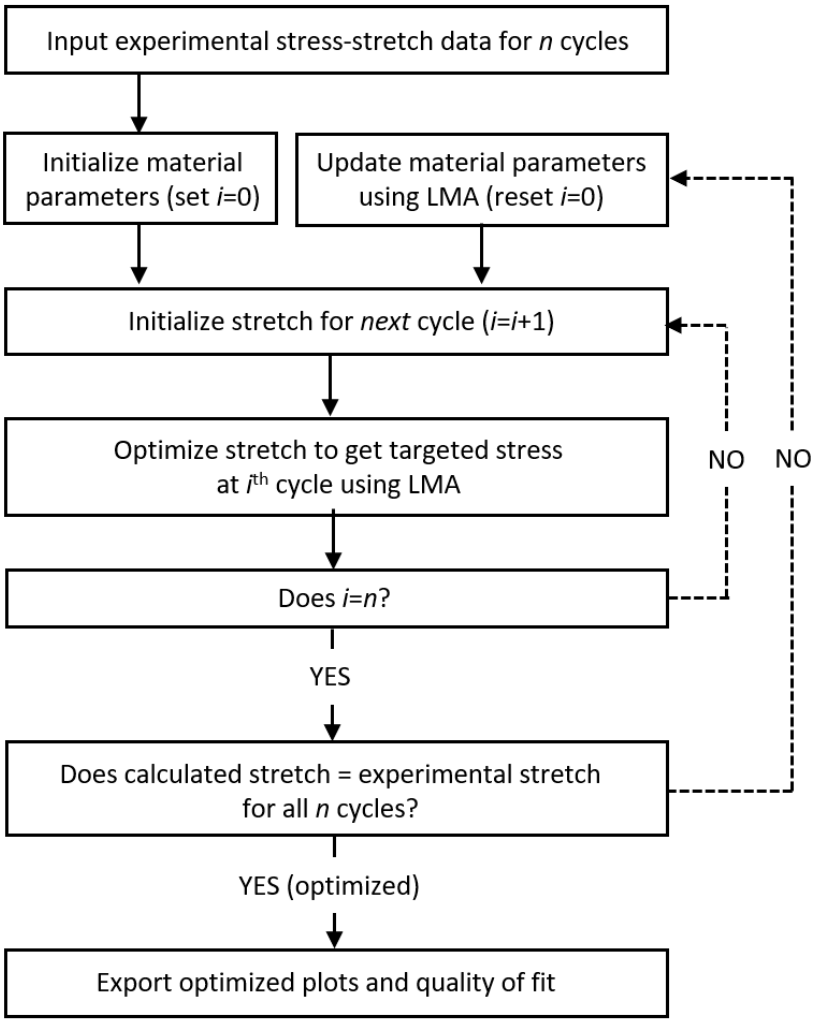

Figure 8. Logic of FC-Opt program. The inner loop indicates (dashed line) the optimization of the resulting axial and lateral stretch values using the Levenberg-Marquardt algorithm (LMA) while the outer loop (dashed line) indicates the optimization of material parameters.

3.2.5 Verification of FC-Opt Program Using a FEBio Comparison

Verification is the process of testing to ensure that the constitutive equations are mathematically implemented correctly (Anderson et al., 2007). This is typically completed through comparison to an analytical solution or an already verified source. The FC-Opt program was verified by comparing its results to the open-source FE solver FEBio (Maas et al., 2012), using the same constitutive equations and material parameters under a force-control ramp (Figure 9). The FE model included a single element hexahedral model with a rigid body connected to the top face, using a sliding elastic contact, to allow displacement along the axial load direction. The Poisson's ratio was set to 0.499 to model incompressibility. A load curve that ramped to 0.25 and then held, was input, and the resulting stretch was compared to the stretch calculated using FC-Opt. For the visco-damage model, the material parameters were selected as E = 5, $\gamma_1 = 3$, $\gamma_2 = 0$, $\gamma_3 = 0$, $\tau_1 = 5$, $\tau_2 = 0$, $\tau_3 = 0$, α = 1, and μ = 0.5. The material parameters relating to the viscoelastic portion of the model were held constant for the viscoelastic verification while the damage parameters α and μ were set to 10,000 so that damage effects were negligible. The numerical models were determined to be successfully verified due to their ability to recreate the data generated using FEBio (Figure 9).

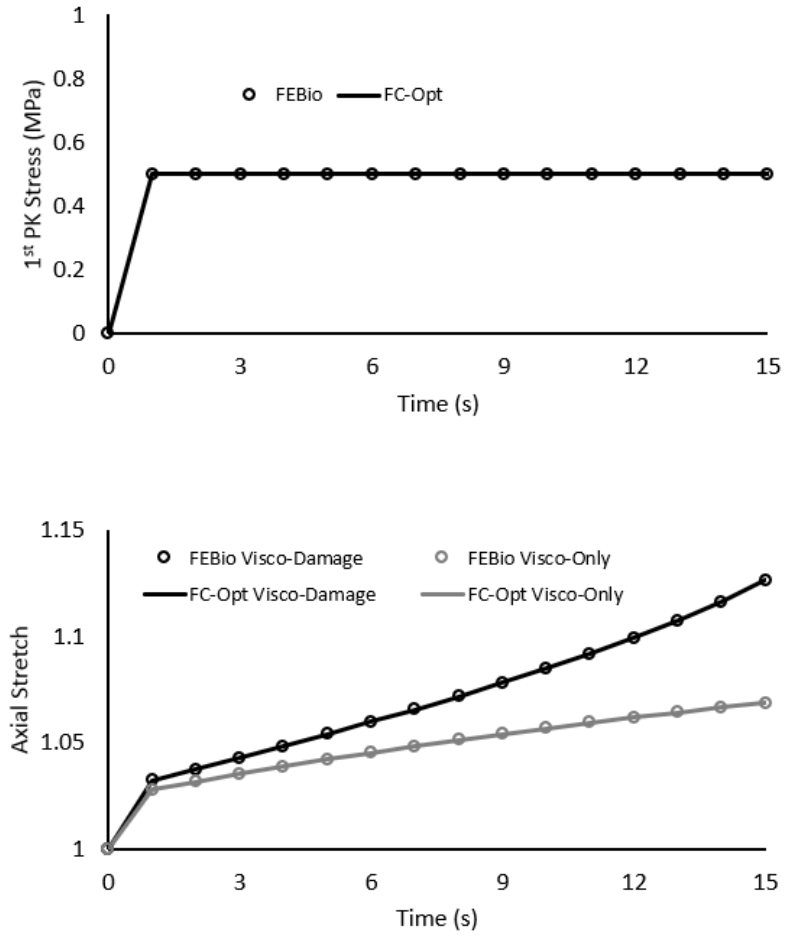

Figure 9. Verification of the mathematics used in the FC-Opt program using FEBio. The input stress indicated on top with the resulting axial stretch for both the visco-damage and visco-only models on bottom.

3.2.6 Validation of FC-Opt Program to Quasi-Static Pull to Failure Experiments

To test the models' ability to represent experimental data that was not used to calibrate the material parameters for fatigue, the viscoelastic-damage model was used to produce quasi-static pull to failure curves. The parameters fit to the fatigue data, for the 70, 50, and 30% stress levels, were applied to the viscoelastic-damage model and fabricated stretch values were input. The resulting stress-stretch responses were then plotted and compared to a range of average ± standard deviation pull to failure experimental data to determine the models' validation (Figure 10).

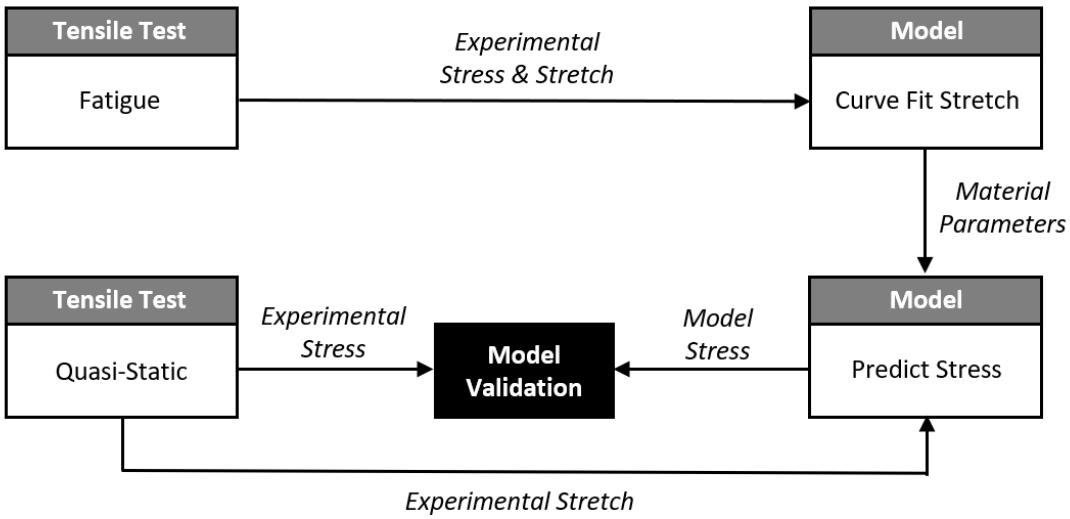

Figure 10. Summary of methods flowchart showing experimental testing, material parameter optimization, mechanical behavior prediction, and model validation.

3.2.7 Sensitivity Analysis of Material Parameters

The sensitivity of the creep curve to each parameter was evaluated using the visco-damage model and a representative test case. For this analysis, each parameter for the elastic and damage terms, including E, α, and μ, were independently increased and decreased by 10% of their optimized value and then plotted for comparison. For the sensitivity analysis regarding the viscoelastic terms, all terms relating to viscoelasticity including γ_1, γ_2, γ_3, τ_1, τ_2, and τ_3 were increased and decreased by 10% of their optimized values and then plotted for comparison.

To evaluate the sensitivity of the constitutive formulation to the number of viscoelastic parameters used, the visco-damage model was reoptimized for two additional cases. For the first case, the model only included 4 viscoelastic terms γ_1, γ_2, τ_1, and τ_2. For the second case, the model only included two viscoelastic terms γ_1 and τ_1. Each case was reoptimized and plotted in comparison to the visco-damage model used in the study

which utilized six viscoelastic terms. RMSE values were then calculated for all three cases.

3.2.8 Statistics

The quality of model fit to the experimental data was evaluated using NRMSE values for each stage of creep (I, II, and III), the total creep (I - III), and the total stress (I - III). The NRMSE values were calculating by dividing the RMSE value of each section by the mean value for that section's experimental data set (e.g. stretch data).

An ANOVA was performed using SPSS (IBM Corp. Released 2017. IBM SPSS Statistics for Macintosh, Version 25.0. Armonk, NY: IBM Corp) for each stage of creep (I, II, and III), the total creep (I - III), and the total stress (I - III) to assess the effect of the model type on the resulting NRMSE values. For all ANOVA tests, a Games-Howell post hoc test was used. A t-test for equality of means was performed to assess the effect of failure occurrence on the maximum damage. All significance levels were set as $p<0.05$.

3.3 Results

The fatigue tests produced characteristic creep curves (stretch versus time) for the force-controlled fatigue loading (Figure 11, 12, and 13). Specimens ruptured before one-million cycles in all but two fatigue experiments in the 30% stress group (Figure 11). For all tests, the median number of cycles to rupture was 74,966 and the average creep rate per one thousand cycles was 0.017%.

In general, the visco-damage model resulted in excellent fits for all three stages of fatigue for all experiments (Figure 11, 12, and 13). One exception was that the visco-damage model had a relatively poor fit to a 30% test that failed before one-million cycles (Figure 11). In comparison, the damage-only model was unable to simulate the steady-

state creep behavior in stage II, and the visco-only model was unable to simulate the failure propagation behavior in stage III. This qualitative observation was supported by quantitative analysis (Table 1). On average, the resulting NRMSE values for stretch at all fatigue stages were 0.22, 2.03, and 0.45% for the visco-damage, damage-only, and visco-only models, respectively (Table 1). The NRMSE values for stage I - III were significantly less for both the visco-damage and visco-only models than the damage-only model (Table 1, $p=0.004$, $p=0.009$, respectively), but were not significantly different between the visco-damage and visco-only models ($p=0.185$).

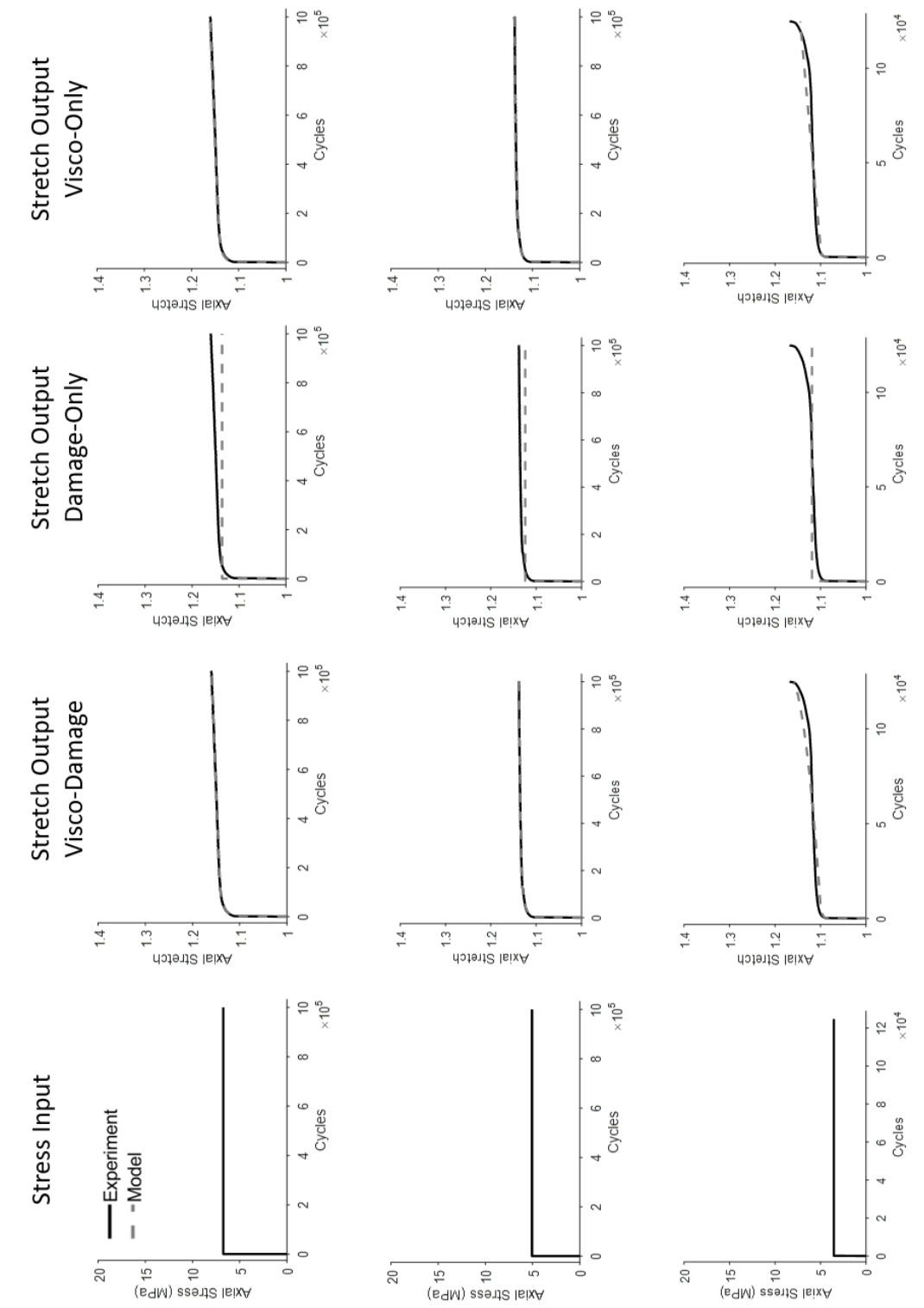

Figure 11. Curve-fit results for the 30% stress level for each model.

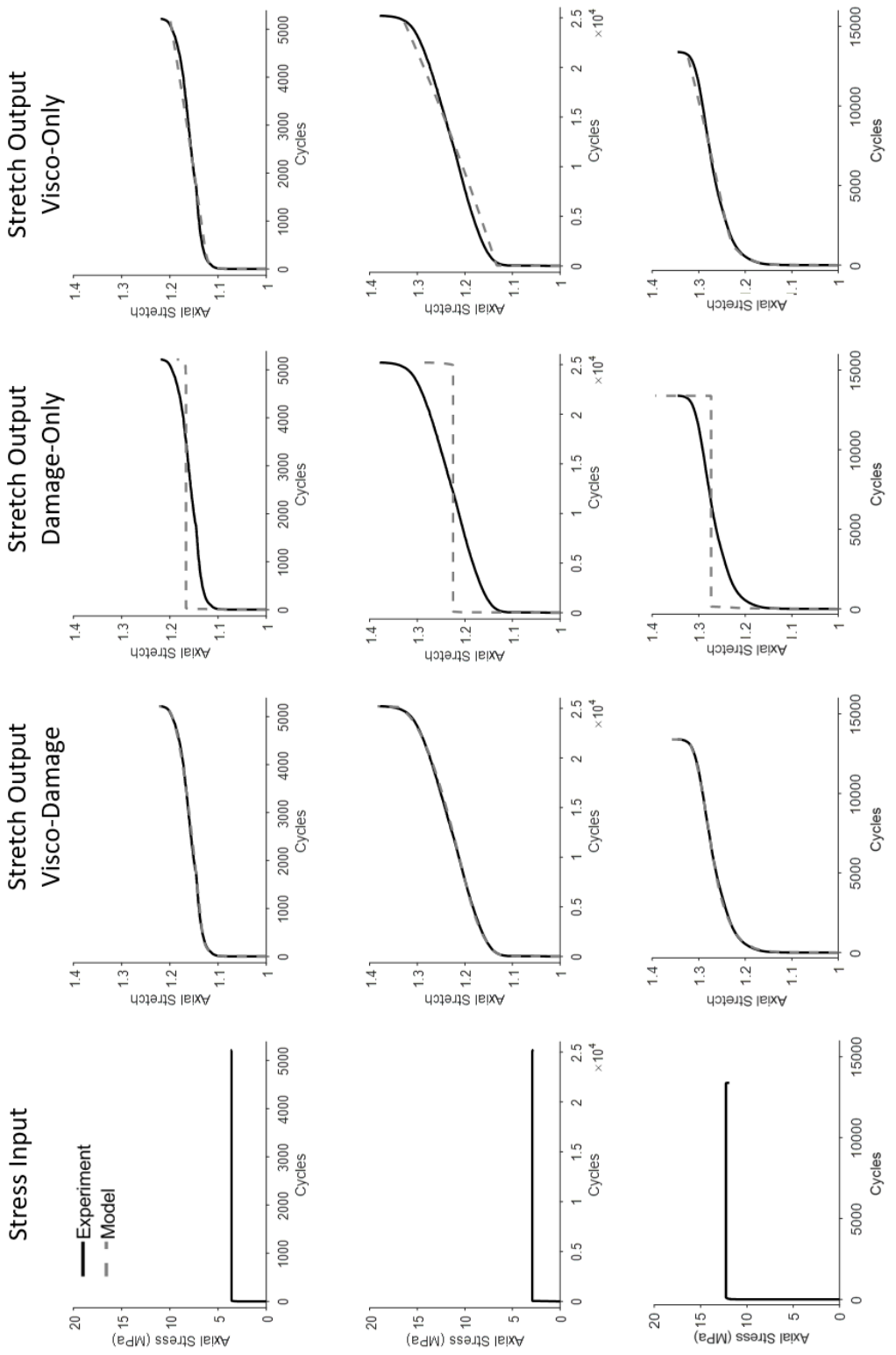

Figure 12. Curve-fit results for the 50% stress level for each model.

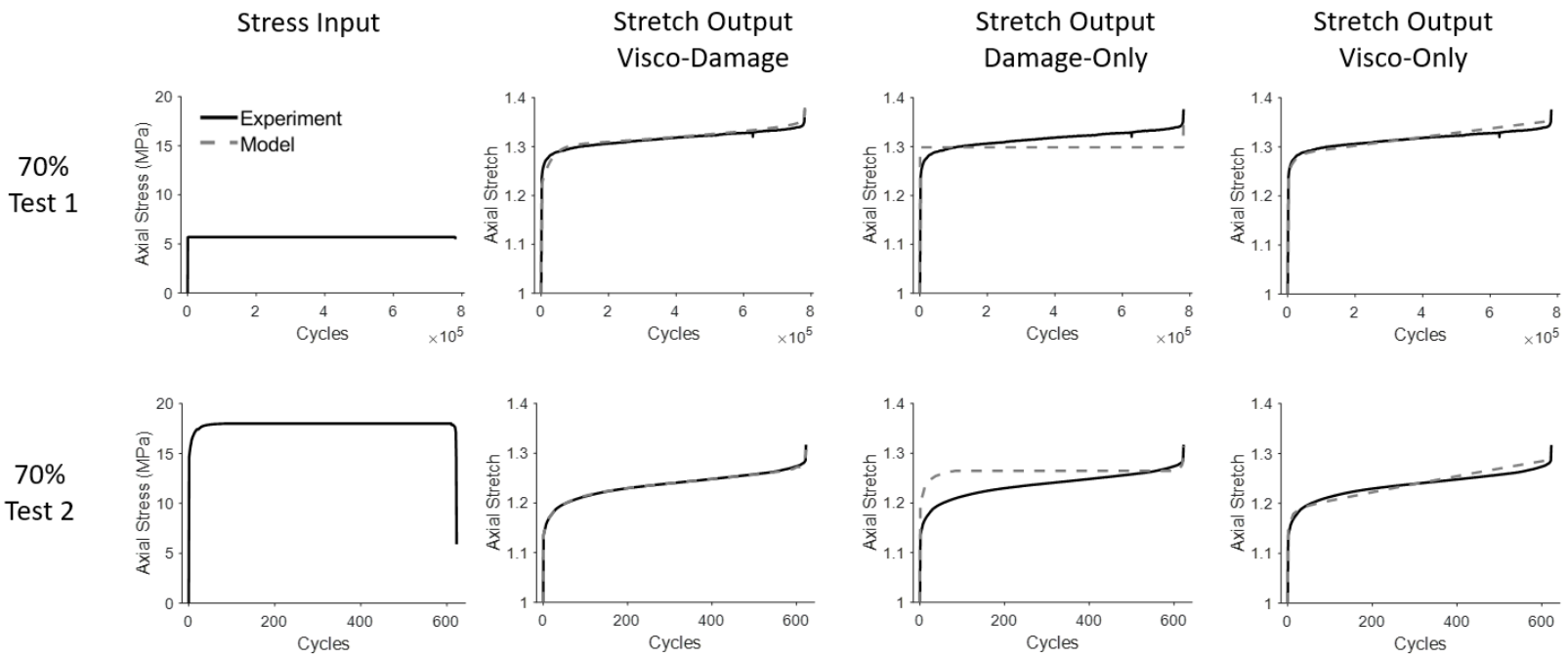

Figure 13. Curve-fit results for the 70% stress level for each model. One experiment was excluded due to irregular stress behavior that could not be modeled with the FC-Opt program.

Table 1. Percent NRMSE values for each model fit at the three different stretch stages of creep (stage I , II , and III) and the percent NRMSE values for each model fit for the total stretch and stress behavior (stretch stage I - III, stress stage I - III). Mean and standard deviation (SD) are shown with values significantly less than the damage-only model indicated (* = p<0.05).

Test	Stretch (Stage I)			Stretch (Stage II)			Stretch (Stage III)			Stretch (Stage I-III)			Stress (Stage I-III)		
	Visco-Damage	Damage-Only	Visco-Only	Visco-Damage	Damage-Only	Visco-Only	Visco-Damage	Damage-Only	Visco-Only	Visco-Damage	Damage-Only	Visco-Only	Visco-Damage	Damage-Only	Visco-Only
30% - 1	0.07	0.68	0.12	0.04	0.65	0.04	0.03	1.46	0.07	0.04	1.31	0.08	0.0	0.0	0.0
30% - 2	0.09	0.50	0.08	0.04	0.69	0.06	0.02	1.05	0.05	0.04	0.96	0.06	0.0	0.0	0.0
30% - 3	0.52	1.34	0.44	0.45	0.37	0.46	0.89	1.58	0.72	0.59	0.94	0.53	0.0	0.0	0.0
50% - 1	0.28	3.44	0.43	0.12	1.32	0.39	0.11	2.06	0.49	0.15	1.90	0.42	0.0	0.0	0.1
50% - 2	0.20	5.95	1.10	0.15	2.94	0.86	0.35	7.02	0.97	0.18	4.06	0.91	0.1	0.2	0.3
50% - 3	0.59	4.79	0.53	0.10	1.28	0.32	0.10	2.92	0.62	0.27	2.56	0.42	0.0	0.1	0.3
70% - 1	0.77	1.40	0.35	0.27	1.75	0.52	0.60	3.14	0.85	0.42	1.81	0.52	0.0	0.2	0.4
70% - 2	0.09	4.52	0.59	0.04	1.82	0.64	0.22	0.50	0.95	0.10	2.66	0.68	0.0	0.0	18.4
Mean	0.33*	2.83	0.45*	0.15*	1.35	0.41*	0.29*	2.47	0.59	0.22*	2.03	0.45*	0.02	0.08	2.43
SD	0.27	2.11	0.32	0.14	0.83	0.28	0.31	2.04	0.36	0.2	1.05	0.29	0.03	0.1	6.44

* Significantly less than Damage-Only (p<0.05)

The models' fits can further be assessed by comparison of each stage of creep. For each stage the visco-damage and visco-only models resulted in significantly less NRMSE values than the damage-only model (Table 1, $p<0.05$) except for stage III where the visco-only model was not significantly different than the damage-only model ($p=0.082$). Further, the visco-damage model had the best fits in each of the three stages compared to the visco-only model, with less than half the NRMSE in stage II and III, although these differences were not significant (Table 1; $p=0.09$, $p=0.25$, respectively). The material parameters determined from curve fitting were reported (Table 2) and the mean and standard deviation were calculated for each model type and stress level (Table 3).

The average maximum damage attained using the visco-damage model was 0.166, 0.291, and 0.345 for the 30, 50, and 70% stress groups, respectively. The average maximum damage using the visco-damage model of the two 30% tests that failure did not occur was 0.0010 and was significantly different ($p=0.016$) from the average of the six tests that did fail, which was 0.344.

The predicted pull to failure results (Figure 14) for each stress group using the visco-damage model resulted in curves that compared well to the average experimental response. Each curve had a qualitative modulus and ultimate tensile strength that was in or close to the range of the experimental data (Figure 14). For the six tests that failed, the average predicted UTS was 11.0 ± 6.8 MPa and was within 40.1% +/- 24.9% of the experimental average. The average predicted failure stretch was 1.27 +/- 0.07 and was within 10.63% +/- 6.21% of the experimental averages for all stress levels.

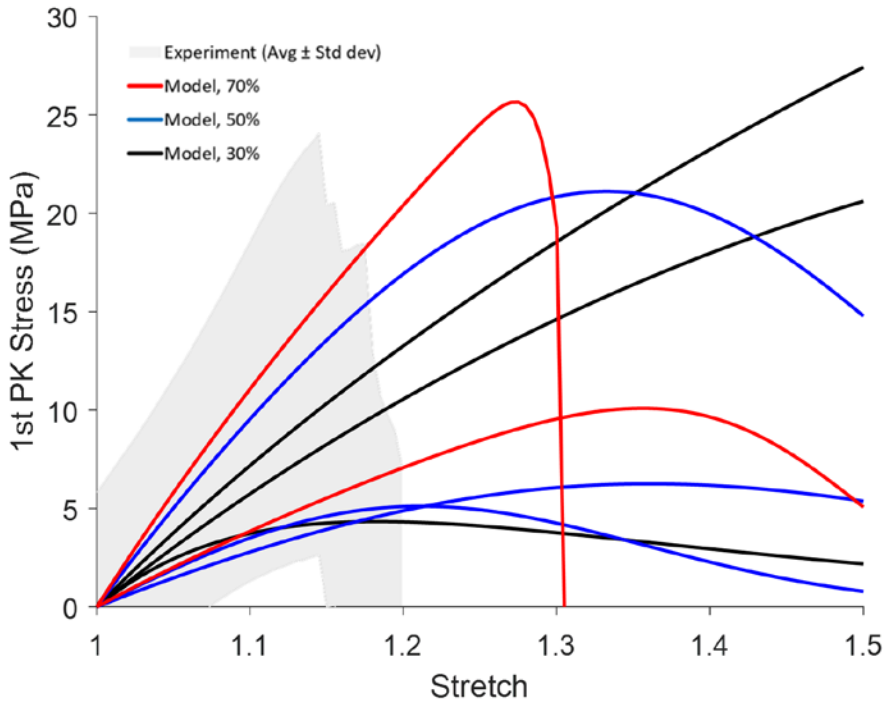

Figure 14. Validation of the visco-damage model applied to the 70, 50, and 30% fatigue tests groups and compared to the range of average quasi-static pull to failure data plus or minus standard deviation determined from 8 experiments performed on specimens obtained from the same knees as the specimens used for fatigue testing.

Table 2. Curve-fit material parameters for each model type and stress level.

Model Type	Test	E (MPa)	Υ_1	τ_1 (s)	Υ_2	τ_2 (s)	Υ_3	τ_3 (s)	α	$\mu\left(\sqrt{\frac{J}{m^3}}\right)$
Visco-Damage	30% - 1	38.0	0.32	109	0.30	5500	0.45	500000	4.03	8.58
	30% - 2	41.1	0.30	140	0.16	9000	0.08	123150	3.05	6.69
	30% - 3	26.0	0.11	467	0.00	9600	1.29	106176	1.12	1.07
	50% - 1	22.1	0.26	26	0.00	556	0.56	1777	2.72	1.41
	50% - 2	9.3	0.56	30	0.51	379	1.24	6629	2.86	1.53
	50% - 3	56.0	0.47	34	0.21	306	0.20	4109	3.55	3.39
	70% - 1	21.0	0.51	85	0.30	5000	0.19	500000	7.01	2.00
	70% - 2	44.6	0.36	13	0.13	10	1.23	434	29.36	1.90
Damage-Only	30% - 1	99.8	0	0	0	0	0	0	0.69	2.87
	30% - 2	497.3	0	0	0	0	0	0	0.16	0.01
	30% - 3	97.8	0	0	0	0	0	0	0.11	0.55
	50% - 1	39.7	0	0	0	0	0	0	1.99	1.48
	50% - 2	29.9	0	0	0	0	0	0	1.37	1.58
	50% - 3	310.8	0	0	0	0	0	0	0.51	1.55
	70% - 1	32.0	0	0	0	0	0	0	3.08	2.34
	70% - 2	87.9	0	0	0	0	0	0	21.58	2.67
Visco-Only	30% - 1	37.0	0.46	100	0.25	5500	0.49	500000	10000	10000
	30% - 2	41.7	0.26	125	0.14	4100	0.11	44748	10000	10000
	30% - 3	10.9	0.02	0	0.65	114	2.62	49995	10000	10000
	50% - 1	0.1	34.87	19	223.49	2428	0.50	4627	10000	10000
	50% - 2	0.0	2336	7139	16070	4658	3460	18081	10000	10000
	50% - 3	0.0	10714	9532	40507	0	4183	90	10000	10000
	70% - 1	12.1	1.01	150	0.28	4143	1.08	500013	10000	10000
	70% - 2	50.8	1.21	169	9.53	0	427.13	0	10000	10000

Table 3. Mean and standard deviation (SD) values for curve-fit material parameters for each model type and stress level.

	Model Type	Test	E (Mpa)	Υ_1	τ_1 (s)	Υ_2	τ_2 (s)	Υ_3	τ_3 (s)	α	$\mu\left(\sqrt{\frac{J}{m^3}}\right)$
Mean	Visco-Damage	30	35.0	0.24	239	0.15	8033	0.60	243109	2.74	5.44
		50	29.1	0.43	30	0.24	413	0.66	4172	3.04	2.11
		70	32.8	0.44	49	0.22	2505	0.71	250217	18.18	1.95
	Damage-Only	30	231.6	0	0	0	0	0	0	0.32	1.14
		50	126.8	0	0	0	0	0	0	1.29	1.53
		70	60.0	0	0	0	0	0	0	12.33	2.50
	Visco-Only	30	29.9	0.25	75	0.35	3238	1.07	198248	10000	10000
		50	0.1	4361.84	5563	18933.31	2362	2547.76	7599	10000	10000
		70	31.5	1.11	160	4.90	2071	214.10	250006	10000	10000
SD	Model Type	Test	E (Mpa)	Υ_1	τ_1 (s)	Υ_2	τ_2 (s)	Υ_3	τ_3 (s)	α	$\mu\left(\sqrt{\frac{J}{m^3}}\right)$
	Visco-Damage	30	8.0	0.12	198	0.15	2214	0.62	222636	1.48	3.91
		50	24.1	0.15	4	0.26	129	0.53	2426	0.45	1.11
		70	13.3	0.16	46	0.11	2878	0.60	288533	14.57	0.05
	Damage-Only	30	230.1	0	0	0	0	0	0	0.32	1.52
		50	159.4	0	0	0	0	0	0	0.74	0.05
		70	39.5	0	0	0	0	0	0	13.08	0.23
	Visco-Only	30	16.6	0.22	66	0.27	2794	1.36	261338	0	0
		50	0.1	5620.50	4948	20293.75	2330	2235.42	9357	0	0
		70	27.4	0.14	14	6.54	2929	301.26	353563	0	0

The sensitivity analysis results show that all parameters, including the elastic modulus, the combined viscoelastic parameters, and both damage parameters affect when failure occurs (Figure 15). For all parameters tested, a decrease in the parameter value resulted in failure at a lower cycle count than the optimized values (Figure 15). The opposite trend was seen when the parameter was increased, such that failure did not occur for the test case studied. Further, the modulus and combined viscoelastic parameters influenced the initial response shown in stage I of the creep curve. When either the modulus or the viscoelastic parameters were decreased, the initial response increased, and when either was increased, the initial response decreased (Figure 15 A,B). This response was not seen when changing either damage parameters as they both had little to no effect on the initial response (Figure 15 C,D).

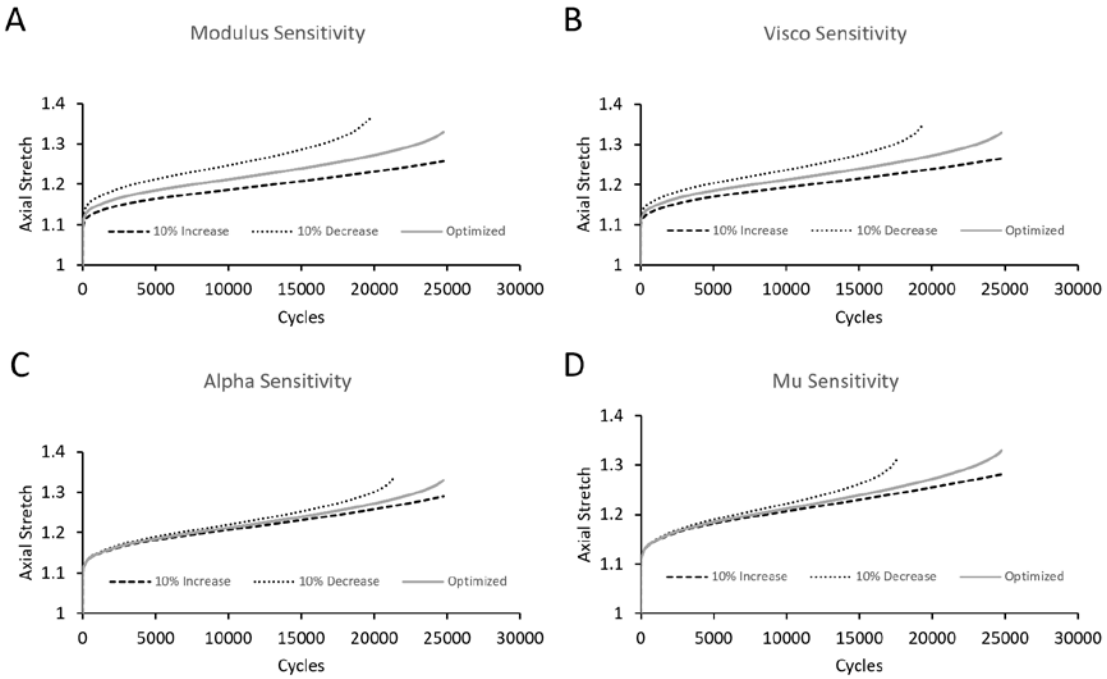

Figure 15. Material parameter sensitivity analysis showing the effect of a 10% increase and decrease for the A) elastic modulus parameter E, B) all six viscoelastic parameters (γ_1, γ_2, γ_3, τ_1, τ_2, and τ_3), C) the damage parameter α, and D) the damage parameter μ for a representative test case with comparison to the optimized curve.

The sensitivity analysis of the visco-damage formulation and the number of viscoelastic parameters indicates that increased parameters improve the model's fit to the experimental data (Figure 16). This is best seen when the model is reduced to only include two viscoelastic terms where the creep behavior cannot be described in all stages. The fit is then improved by adding two more parameters where the creep curvature is better fit (Figure 16). Lastly, two more viscoelastic parameters are added for a total of six, which was the amount used for the visco-damage model, and the fit results are further improved and can model all three creep stages (Figure 16). These qualitative observations were further supported with quantitative analysis. The RMSE values of each case when compared to the experimental stretch values were 0.65, 0.23, and 0.19% for the 2 term, 4 term, and 6 term cases, respectively.

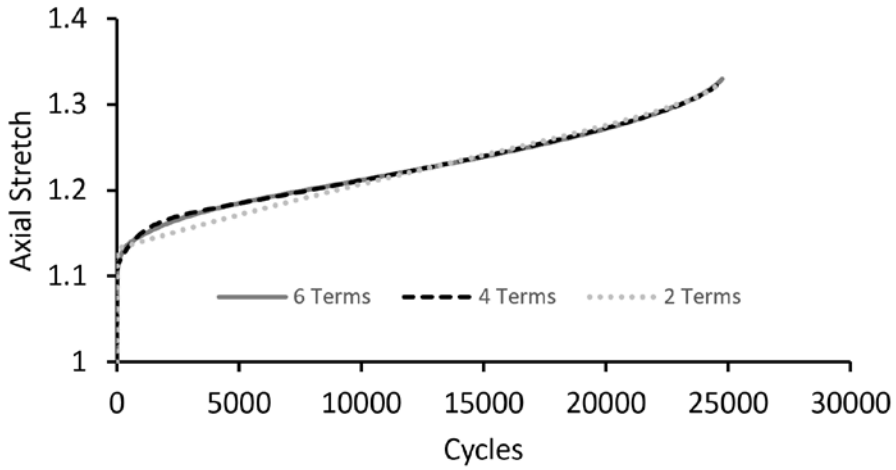

Figure 16. Sensitivity to the number of visco-elastic terms used in the visco-damage constitutive model. The resulting creep curves are plotted for a visco-damage model that included 6, 4, and 2 viscoelastic terms defining the relaxation function. The analysis indicates that increasing the number of viscoelastic terms improves the quality of fit.

3.4 Discussion

This study demonstrates for the first time the feasibility of using a visco-damage formulation to model the creep response of soft fibrous tissue during force-control cyclic fatigue loading. Moreover, this study was able to reproduce a range of time-dependent, non-linear, fatigue behavior with a neo-Hookean viscoelastic model and a rather simple discontinuous damage evolution equation that had only two material parameters. These results support our hypothesis and highlight the importance of pairing both viscoelasticity and damage formulations when modeling fatigue induced creep.

The effectiveness of the visco-damage model was due to the selection of an energy-based damage criteria that enabled viscoelastic creep to drive damage evolution, even during constant stress. This can be better understood by examining the three unique regions of the cyclic strain curve (Figure 5). As the material is initially loaded in stage I, an increase in stress and stretch will effectively cause material weakening due to the strain-energy damage threshold being exceeded. Once stress becomes constant in phase II, the gradual steady-state increase in stretch is regulated by the time-dependent terms in the viscoelastic model. Importantly, the incremental increases in stretch from viscoelasticity will continue to evolve damage, until increases in strain energy eventually cause stage III, where stretch values quickly rise until tissue rupture. By comparison, when using the visco-only model, stage II could be reasonably fit, but the visco-only model could not fit the exponential increase in stretch observed in stage III (Figure 11-13). Conversely, when using the damage-only model, the exponential increase in stretch in stage III could be modeled, but the steady-state response during constant stress in stage II could not be modeled, as damage does not evolve (Figure 11-13). The visco-damage

model was unique in having good fits for stage I, II, and III (NRMSE = 0.33, 0.15, 0.29%, respectively).

The damage levels predicted by the models give insight into the failure mechanics of the tissue. For experiments that did not fail, the energy was maintained below a threshold where damage did not evolve, and the response was purely viscoelastic. This indicates the possibility of an endurance limit where damage will not develop and at which failure will never occur regardless of cycle count. For experiments that did fail, low levels of damage, ranging from 0.05 to 0.2, resulted in an exponential increase in stretch. This indicates that under force-controlled fatigue, soft tissues may experience a catastrophic failure without a considerable accumulation of damage (Figure 17).

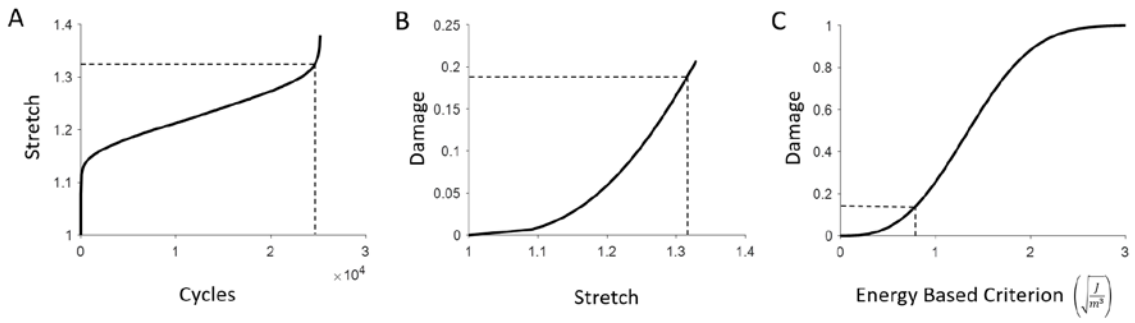

Figure 17. Representation of low damage levels resulting in an exponential increase in stretch leading to tissue rupture. A) Stretch versus cycles data for the viscoelastic-damage model with corresponding plots for B) damage versus stretch and C) damage versus the Simo damage criteria.

The material parameters give insight into the physiological accuracy of the model. Quasi-static pull to failure experiments performed before fatigue testing resulted in modulus values ranging from 26.2 to 197.7 MPa (Figure 14). On average, both the visco-damage and damage-only models resulted in modulus values close to the experimental range. In contrast, the visco-only model resulted in modulus values much lower for the 50% stress level (Table 3). This is likely due to this model amplifying the elastic response

by under predicting the modulus and then relaxing to the long-term elastic behavior. The study further showed that the visco-damage formulation was sensitive to all material parameters utilized and that the selection of six viscoelastic terms resulted in the best fit in comparison to visco-damage models with reduced terms.

This study developed a program that can successfully optimize material parameters for force-controlled loading. The original intent of this study was to apply the constitutive equations in a FE solver, however, major limitations regarding modeling of force-controlled damage were discovered. The newton-based solvers in FE frameworks use the slope of the stress-strain behavior to determine the future solution (FEBio, n.d.). If softening due to damage occurs too quickly and becomes localized in a narrow band of elements, the slope may approach zero resulting in the model diverging (FEBio, n.d.). A potential solution to this limitation is using a regularized softening modulus that defines the total amount of dissipated energy preventing the localization of damage. However, open-source FE solvers are still unable to optimize material parameters for a force-controlled load. FE solvers can optimize material parameters in displacement-control for fatigue (Henderson et al., 2020), but these parameters are not compatible when simulating the experiment in force-control. This study overcame these inherent limitations of FE solvers by utilizing a least-squares approach in a custom program. This FC-Opt program allowed for modeling force-controlled damage with material parameter optimization by minimizing the difference between the experimental and predicted stress at various stretch values. Further, the FC-Opt program's ability to optimize material parameters and predict stretch values correctly was verified using the open-source FE

solver FEBio (Figure 9). The FC-Opt program compared very well to FEBio for a force-controlled ramp using both the visco-damage and visco-only constitutive equations.

Although verification of models is necessary to ensure mathematical correctness, it is still required to test the model's ability to recreate data that was not used for material parameter determination through validation (Anderson et al., 2007). The validation results indicate that the visco-damage formulation was able to predict specimen specific modulus values and ultimate tensile strengths that compare well with average quasi-static pull to failure experiments (Figure 14). However, the stretch values at failure suggest that damage could be underpredicted in the model utilized or that fatigue could be more resistant to damage than pull to failure loading (Figure 14). These results also suggest that the Neo-Hookean elastic model utilized by the FC-Opt program is not sufficient in predicting the non-linear stress-stretch response of the meniscus tissue.

Previous studies that have modeled soft tissue damage for cyclic loading have used a discontinuous CDM formulation. In Balzani et al., (2012) a constitutive framework is proposed to describe stress softening due to cyclic loading in collagenous soft tissue and was applied to arterial walls. Further, Pena, (2011) predicted the uniaxial stress response under cyclic loading including softening, damage effects, and permanent set in fibrous biological materials using two weight factors and discontinuous damage. However, these studies like several others do not focus on modeling long-term fatigue behavior. Martin and Sun, (2012) addressed this gap by introducing a model to describe cyclic fatigue damage in soft tissue using a continuous damage formulation that was dependent on both the equivalent strain and the loading cycles. This description assumes a linear progression of stress softening as a function of the number of loading cycles and

was only applied to displacement-controlled loading. The linear approximation is not characteristic of force-controlled creep given that damage may evolve faster in the initial loading cycles and failure regions. The rational of the constitutive formulation utilized in this study for modeling the long-term force-controlled fatigue behavior of meniscus tissue is the ability to model all three stages of creep including rupture. The present study also shows that a more conventional discontinuous damage criteria paired with viscoelasticity can effectively be applied providing a more physiological description of the material's behavior. Further, the validation results of this study indicate that the visco-damage formulation shows potential in modeling fatigue and static failure simultaneously in contrast to the continuous damage formulation presented by Martin and Sun, (2012) that is cycle dependent and thus not suitable for static failure.

This study has several limitations. The model used a single volumetric element to describe the material behavior and did not account for specimen geometry or local behavior. However, the single element model still leads to insights regarding experimental behavior and shows the feasibility of this novel modeling approach. The model also implemented a constraint that axial stretch could not decrease to enforce the condition that damage is irreversible. This contributed to the increase in damage observed in stage III for both the visco-damage and damage-only models due to the experimental force reduction. This assumption has validity for stress-control experiments but is not a direct physical representation of what might occur naturally and may cause limitations when modeling other loading scenarios. Further, the model could not represent experiments with a prolonged stage III, as shown by test 30% - 3. This test case's limited viscoelastic response in stage II confines the evolution of damage. Lastly, the elastic

model is not representative of the tissue structure and results in insufficient validation. The isotropic, Neo-Hookean formulation has a limited ability to model the non-linear response of soft tissue during quasi-static pull to failure loading, however; this model was very effective in modeling for fatigue loading. Future studies should apply a transversely isotropic model, that is more representative of meniscus' non-linear stress response (Pena, 2011), using experimental data for both transverse and longitudinal directions for material parameter determination.

For the first time, this study has identified a constitutive equation capable of modeling force-controlled cyclic creep to failure in soft tissue. Future work will advance this model by using an elastic formulation more representative of the meniscus tissue's structure. The outer loop of the FC-Opt program could then be implemented into a FE solver to optimize material parameters, further describing the mechanical characteristics of force-controlled fatigue in human meniscus tissue. The findings of this study progress the mechanical knowledge of force-controlled fatigue in soft tissues and are applicable in the prediction and prevention of meniscus tissue injuries.

CHAPTER FOUR: CONCLUSIONS

4.1 Summary

The research goal was to determine a constitutive model that is effective in describing the creep response of human meniscus tissue to force-controlled fatigue loading. To accomplish this objective three constitutive models were utilized including a viscoelastic damage model, a continuum damage mechanics model, and a viscoelastic model in attempts of reproducing experimental results.

- To our knowledge, this is the first study to model creep behavior due to force-controlled fatigue loading in meniscus or any other soft tissue.
- The visco-damage model best simulated the force-controlled fatigue induced creep behavior in human meniscus tissue.
- Damage could not independently represent the entire creep behavior, as damage did not accumulate through the steady-state creep phase (stage II).
- Viscoelasticity could not independently represent the entire creep behavior, as viscoelasticity could not model the exponential creep phase to failure (stage III).
- The maximum damage produced by the visco-damage model was significantly different for experiments that did and did not fail. Further, low amounts of damage resulted in massive increases in stretch indicating that force-controlled fatigue may result in catastrophic failure without large accumulations of damage.
- The combination of discontinuous CDM and viscoelasticity shows potential in modeling both static and fatigue loading using a single formulation.

4.2 Limitations

The study presented has several limitations. The program implemented a single element model representing the tissue's behavior; thus, it cannot describe or predict phenomena caused by specimen geometry that may further insights into the tissue's failure mechanics. The isotropic model used is also not representative of the fibrous tissue structure. Consequently, the material parameters predicted by the model represent a combination of the meniscus fibers and ground matrix, which have been shown to display different properties. Further, the elastic model and the resulting material parameters from this study could not represent average stress-strain meniscus tissue data. This is likely due to the Neo-Hookean formulation's limited ability to describe non-linear behavior. The program also constrained the determined stretch data to be equal or greater than the previous data point to ensure the damage was irreversible. This is not representative of natural loading and may limit the model's application to other loading scenarios. The study also only looked at one type of relaxation function used to model viscoelasticity and only one type of damage criteria and CDF to model damage, thus other model formulations may be able to model the studied behavior more effectively. Lastly, the model showed limitation in representing creep behavior with a prolonged stage III.

4.3 Future Work

To improve upon the current study and address the limitations presented, the outer loop of the program developed could be implemented into a FE solver to optimize material parameters for force-controlled loading. The parameters determined could then be implemented to further describe the tissue’s behavior. Further, the constitutive

formulations could be adapted to represent the material's transversely isotropic structure. Parameters could then be fit for both the fibers and the ground matrix to axial and transverse fatigue data. Lastly, an elastic model better suited to represent non-linear stress-strain behavior must be implemented to improve validation.

REFERENCES

Anderson, A. E., Ellis, B. J., & Weiss, J. A. (2007). Verification, validation and sensitivity studies in computational biomechanics. *Computer Methods in Biomechanics and Biomedical Engineering, 10*(3), 171-184. doi:10.1080/10255840601160484

Balzani, D., Brinkhues, S., & Holzapfel, G. A. (2012). Constitutive framework for the modeling of damage in collagenous soft tissues with application to arterial walls. *Computer Methods in Applied Mechanics and Engineering, 213-216*, 139-151. doi:10.1016/j.cma.2011.11.015

Bullough, P., Munuera, L., Murphy, J., Weinstein, A., & Smith, N. (1970, August 01). The Journal of Bone and Joint Surgery. British volume. Retrieved November 18, 2020, from https://online.boneandjoint.org.uk/doi/abs/10.1302/0301-620x.52b3.564?journalCode=bjj

Clark, C. R., & Ogden, J. A. (1983). Development of the menisci of the human knee joint. Morphological changes and their potential role in childhood meniscal injury. *The Journal of Bone & Joint Surgery, 65*(4), 538-547. doi:10.2106/00004623-198365040-00018

Creechley, J. J., Krentz, M. E., & Lujan, T. J. (2017). Fatigue life of bovine meniscus under longitudinal and transverse tensile loading. *Journal of the Mechanical Behavior of Biomedical Materials, 69*, 185-192. doi:10.1016/j.jmbbm.2016.12.020

Demange, M. K., Gobbi, R. G., & Camanho, G. L. (2015). “Fatigue meniscal tears”: A description of the lesion and the results of arthroscopic partial meniscectomy. *International Orthopaedics, 40*(2), 399-405. doi:10.1007/s00264-015-3010-5

Edd, S. N., Giori, N. J., & Andriacchi, T. P. (2015). The role of inflammation in the initiation of osteoarthritis after meniscal damage. *Journal of Biomechanics*, *48*(8), 1420-1426. doi:10.1016/j.jbiomech.2015.02.035

FEBio. (n.d.). Retrieved November 18, 2020, from https://help.febio.org/FEBio/FEBio_um_2_8/

Fox, A. J., Bedi, A., & Rodeo, S. A. (2012). The Basic Science of Human Knee Menisci. *Sports Health: A Multidisciplinary Approach*, *4*(4), 340-351. doi:10.1177/1941738111429419

Franceschini, G., Bigoni, D., Regitnig, P., & Holzapfel, G. (2006). Brain tissue deforms similarly to filled elastomers and follows consolidation theory. *Journal of the Mechanics and Physics of Solids, 54*(12), 2592-2620. doi:10.1016/j.jmps.2006.05.004

Henderson, B. S., Cudworth, K. F., Siegel, D. N., Krentz, M. E., Pena, E., & Lujan, T. J. (2020). Model Fatigue Failure in Fibrous Soft Tissue [Abstract].

Herwig, J., Egner, E., & Buddecke, E. (1984). Chemical changes of human knee joint menisci in various stages of degeneration. *Annals of the Rheumatic Diseases, 43*(4), 635-640. doi:10.1136/ard.43.4.635

Hoshino, A., & Wallace, W. (1987). Impact-absorbing properties of the human knee. *The Journal of Bone and Joint Surgery. British Volume, 69-B*(5), 807-811. doi:10.1302/0301-620x.69b5.3680348

Hutchinson, I. D., Moran, C. J., Potter, H. G., Warren, R. F., & Rodeo, S. A. (2013). Restoration of the Meniscus. *The American Journal of Sports Medicine, 42*(4), 987-998. doi:10.1177/0363546513498503

IBM Corp. Released 2017. IBM SPSS Statistics for Windows, Version 25.0. Armonk, NY: IBM Corp. (n.d.). Retrieved November 15, 2020.

Imeni, M., Seyfi, B., Fatouraee, N., & Samani, A. (2020). Constitutive modeling of menisci tissue: A critical review of analytical and numerical approaches. *Biomechanics and Modeling in Mechanobiology*, *19*(6), 1979-1996. doi:10.1007/s10237-020-01352-1

Jha, N. K., Nackenhorst, U., Pawar, V. S., Nadella, R., & Guruprasad, P. (2019). On the constitutive modelling of fatigue damage in rubber-like materials. *International Journal of Solids and Structures, 159,* 77-89. doi:https://doi.org/10.1016/j.ijsolstr.2018.09.022

Kim, S., Bosque, J., Meehan, J. P., Jamali, A., & Marder, R. (2011). Increase in Outpatient Knee Arthroscopy in the United States: A Comparison of National Surveys of Ambulatory Surgery, 1996 and 2006. *The Journal of Bone and Joint Surgery-American Volume, 93*(11), 994-1000. doi:10.2106/jbjs.i.01618

Kohn, D., & Moreno, B. (1995). Meniscus insertion anatomy as a basis for meniscus replacement: A morphological cadaveric study. *Arthroscopy: The Journal of Arthroscopic & Related Surgery, 11*(1), 96-103. doi:10.1016/0749-8063(95)90095-0

Maas, S. A., Ellis, B. J., Ateshian, G. A., & Weiss, J. A. (2012). FEBio: Finite Elements for Biomechanics. *Journal of Biomechanical Engineering, 134*(1). doi:10.1115/1.4005694

Martin, C., & Sun, W. (2012). Modeling of long-term fatigue damage of soft tissue with stress softening and permanent set effects. *Biomechanics and Modeling in Mechanobiology, 12*(4), 645-655. doi:10.1007/s10237-012-0431-6

Martin, C., & Sun, W. (2017). Fatigue Damage of Collagenous Tissues: Experiment, Modeling and Simulation Studies. *Fatigue Damage of Collagenous Tissues: Experiment, Modeling and Simulation Studies, 25*(1-2), 55-73.

Nelson, S. J., Creechley, J. J., Wale, M. E., & Lujan, T. J. (2020). Print-A-Punch: A 3D printed device to cut dumbbell-shaped specimens from soft tissue for tensile testing. *Journal of Biomechanics, 112,* 110011. doi:10.1016/j.jbiomech.2020.110011

Nesbitt, D. Q., Siegel, D. N., Nelson, S. J., & Lujan, T. J. (2020). Effect of Age on the Failure Properties of Human Meniscus: High-Speed Strain Mapping of Tissue Tears. *Journal of Biomechanics.*

Ogden, R., & Roxburgh, D. (1999). A Pseudo-Elastic Model for the Mullins Effect in Filled Rubber. *Royal Society, 455*(1988), 2861-2877.

Peloquin, J. M., & Elliott, D. M. (2016). A comparison of stress in cracked fibrous tissue specimens with varied crack location, loading, and orientation using finite element analysis. *Journal of the Mechanical Behavior of Biomedical Materials, 57*, 260-268. doi:10.1016/j.jmbbm.2015.12.004

Peña, E. (2011). Prediction of the softening and damage effects with permanent set in fibrous biological materials. *Journal of the Mechanics and Physics of Solids, 59*(9), 1808-1822. doi:10.1016/j.jmps.2011.05.013

Peña, E., Calvo, B., Martínez, M. A., & Doblaré, M. (2007). On finite-strain damage of viscoelastic-fibred materials. Application to soft biological tissues. *International Journal for Numerical Methods in Engineering, 74*(7), 1198-1218. doi:10.1002/nme.2212

Radin, E. L., De, F., & Maquet, P. (1984). Role of the Menisci in the Distribution of Stress in the Knee. *Clinical Orthopedics and Related Research, &NA;*(185). doi:10.1097/00003086-198405000-00047

Roos, E., Östenberg, A., Roos, H., Ekdahl, C., & Lohmander, L. (2001). Long-term outcome of meniscectomy: Symptoms, function, and performance tests in patients with or without radiographic osteoarthritis compared to matched controls. *Osteoarthritis and Cartilage, 9*(4), 316-324. doi:10.1053/joca.2000.0391

Runesson, K. (2006). CONSTITUTIVE MODELING OF ENGINEERING MATERIALS - THEORY AND COMPUTATION. Retrieved November 16, 2020, from http://www.am.chalmers.se/~ragnar/material_mechanics_home/literature/ThePrimer_(1).pdf

Snoeker, B. A., Bakker, E. W., Kegel, C. A., & Lucas, C. (2013). Risk Factors for Meniscal Tears: A Systematic Review Including Meta-analysis. *Journal of Orthopedic & Sports Physical Therapy, 43*(6), 352-367. doi:10.2519/jospt.2013.4295

Sopakayang, R., & Vita, R. D. (2011). A mathematical model for creep, relaxation, and strain stiffening in parallel-fibered collagenous tissues. *Medical Engineering & Physics, 33*(9), 1056-1063. doi:10.1016/j.medengphy.2011.04.012

Sweigart, M. A., & Athanasiou, K. A. (2001). Toward Tissue Engineering of the Knee Meniscus. *Tissue Engineering, 7*(2), 111-129. doi:10.1089/107632701300062697

Total Meniscus Replacement Technology. (2017, December 01). Retrieved November 16, 2020, from http://orthonika.com/total-meniscus-replacement/total-meniscus-replacement-technology

Voloshin, A. S., & Wosk, J. (1983). Shock absorption of meniscectomies and painful knees: A comparative in vivo study. *Journal of Biomedical Engineering, 5*(2), 157-161. doi:10.1016/0141-5425(83)90036-5

Wale, M. E., Nesbitt, D. Q., Henderson, B. S., Fitzpatrick, C. K., Creechley, J. J., & Lujan, T. J. (2020). Applying ASTM Standards to Tensile Tests of Musculoskeletal Soft Tissue: Methods to Reduce Grip Failures and Promote Reproducibility. *Journal of Biomechanical Engineering, 143*(1). doi:10.1115/1.4048646

Zhu, Y. (2018). An elasto-viscoplastic model to describe the ratcheting behavior of articular cartilage. *Biomechanics and Modeling in Mechanobiology, 17*, 1875-1883. doi:10.1007/s10237-018-1062-3